






# A Selective Harmonic Compensation with Current Limiting Algorithm

Nayara V. Oliveira<sup>(✉)</sup> , Cleiton M. Freitas<sup>(D)</sup> , and Luis F. C. Monteiro<sup>(ID)</sup> 

Rio de Janeiro State University, Campus Maracanã,  
Rio de Janeiro, RJ 25550-000, Brazil  
nayvillela@gmail.com, {cleiton.freitas, lmonteiro}@uerj.br

**Abstract.** This paper addresses a control algorithm to determine the reference currents indirectly from the grid voltages, taking into account the limited capacity of the power converter for compensating, entirely, the selected harmonic current. In previous works, the reference current was indirectly determined based on an average component correlated with the selected harmonic current. Thus, when the selected harmonic current was entirely compensated, that average value was decreased to zero. Now, this paper introduces a novel control algorithm considering the limited capacity of the power converter for producing the selected harmonic current. In this novel condition, the phase-angle of the reference current is dynamically modified while the minimum point of the cost function is not reached. The remaining parameters of the reference currents correspond to the harmonic frequency and amplitude as well. The harmonic frequency was identified through a PLL (Phase-Locked-Loop) circuit whereas the amplitude corresponds to a specific value of 10A to all of the developed test cases. Other aspects of the simulated power circuit, control algorithms, including the optimization methods, are described throughout the paper. Simulation results involving different test cases were implemented to verify the performance of the proposed algorithm compensating of the fifth-harmonic component under transient -and steady-state conditions.

**Keywords:** Active filtering · Real-time control algorithms · Optimization methods · Distribution power-grids

## 1 Introduction

Due to the proliferation of nonlinear loads, power quality has been compromised in distribution power grids [1,2]. Indeed, current harmonics cause undesirable effects as, for instance, over heating of cables and transformers, over current in neutral wires and electromagnetic interference (EMI) problems. As alternative to

---

“This study was financed in part by the Coordenação de Aperfeiçoamento de Pessoal de Nível Superior - Brasil (CAPES) - Finance Code 001”.

suppress current harmonics are the use of passive power filters, which has been a preferred solution by consumers once it is considered a low-cost solution in comparison to the existing ones. However, passive filters present several problems as, for example, the resonance phenomena, which leads to over current or over voltage on the grid. An enhanced solution corresponds to the active power filters as mentioned by [3]. Active filters are capable to compensate current harmonics generated by different types of nonlinear loads and power factor as well, with fast transient response.

Active power filters have been researched for decades and, even now, they are of great interest due to the their controlled harmonic mitigation [4–10]. In a general approach, the load currents are measured and their harmonic components are identified to be compensated by the power converter [11]. In this context, the power converter behaves as a very-low impedance path to the harmonic currents produced by nonlinear loads, such that, considering an ideal situation, only the fundamental component flows throughout the grid.

Different current control strategies for active power filters have been reported in the literature, such as adaptive fuzzy control [12], linear feedback control [13] and adaptive observer [14]. As shown by [12], the load -and filter-currents are used as reference for the adaptive fuzzy control to generate the total compensation currents for a nonlinear load. Moreover, in [13] was proposed a linear feedback control based on an iterative learning control algorithm based on adaptive proportional-integral controller (PI) with load reference current and source of the algorithm. In [14] the proposed control was based on an adaptive observer without considering the voltage information at the Point of Common Coupling (PCC). Other possibility was to conceive the control algorithms based on the grid currents instead of the load currents, such that the grid currents are forced to track this fundamental positive-sequence component, with the load current harmonics provided by the active filter in an indirect way [15]. The main advantages of this approach are that only one low-bandwidth current sensor is required, and a faster transient response is achieved [11].

Nevertheless, one may see that all of these aforementioned solutions are based on the load -or grid-currents to determine the reference ones. Furthermore, in radial grids with widespread loads it is not feasible spreading large amount of current transducers so as to detect the variety of loads up and downstream from the active power filters. An alternative consists on swapping the measured-current compensation approach for one in which the compensation currents are computed from the harmonic voltage-drops caused by the harmonic currents flowing through the grid impedance, as proposed by [16–18]. In this approach, a specific harmonic component or even a symmetrical component of the harmonic current is compensated taking into consideration the corresponding harmonic voltage-drop, which is measured at the PCC voltage. Basically, it was calculated a cost function based on the harmonic voltage drop and the reference current was dynamically modified (phase-angle and magnitude) while the average component of this cost function was not decreased to zero. In this condition (average component of the cost function equal to zero) it was assured fully compensation

of the selected harmonic current. However, to meet this condition, the active filter is forced to produce the selected harmonic current drawn by all of the non linear loads, which may become unfeasible once the limited capacity of the power converter was not taken into account. Thus, as a contribution of this paper, this issue was considered which led to a novel control algorithm. Other aspects of the proposed control algorithm are exploited and explained throughout this paper.

The article is organized into four sections. In Sect. 2 there is a general description of the simulated circuit. Sections 3 and 4 exploits the control algorithms and the simulation results, respectively. Finally, conclusions obtained through this work are described in Sect. 5.

## 2 General Circuit Description

In Fig. 1 a simplified electrical scheme of the simulated circuit is shown. It corresponds to a three phase radial grid, 220 V (line-line voltage) and 60 Hz, with the source voltage and the grid impedance labelled as  $v_s$ , and  $Z_s$ , respectively. In this work  $Z_s$  was considered inductive and constant. Nevertheless, currently there is a new concept of the grid impedance being variable, and this issue will be taken into account in our future works. This grid supplies a linear load,  $R_c$ , and a set of unbalanced harmonic loads. Yet, a shunt active power filter is connected to the point of common coupling through a damped LCL circuit. For sake of simplicity the dc-link voltage,  $v_{dc}$ , was considered constant and equal to 1200 V, however, a voltage source was used as it was not the purpose of this paper to carry out the control of the dc-link voltage. Thus, a high voltage source was used for the study in question. Furthermore, as illustrated in Fig. 1 and summarized in Table 1,  $L_1$  and  $L_2$  are coupling inductors and  $Z_c$  is the RC branch, composed by a capacitor  $C_1$  and resistor  $R_1$ , to provide low-impedance path to switching-frequency components.

## 3 Control Algorithms

The simplified block diagrams as it is presented in Fig. 2 depicts the implemented algorithms to determine the reference currents and the produced voltages as well. It is composed by a synchronizing circuit Phase-Locked-Loop (PLL) to extract a control signal ( $\omega t$ ) synchronized with the fundamental positive-sequence component of the grid voltages  $v_{ga}$ ,  $v_{gb}$  and  $v_{gc}$ . Based on the PLL output signal,  $5\omega t$ , together with the grid voltages, the direct -and quadrature-components of the fifth-harmonic (negative-sequence) grid voltages ( $vd_{5h}$  and  $vq_{5h}$ ) are calculated through Park Transformation. In sequence,  $vd_{5h}$  and  $vq_{5h}$  are filtered through a 1<sup>st</sup> order low-pass filter with cut-off frequency of 30 Hz. It is necessary once the grid voltages, in our case study, are comprehended by the fundamental -and fifth-harmonic components. Thus,  $vd_{5h}$  and  $vq_{5h}$  are composed by an average component plus oscillating components at  $4\omega t$  and  $6\omega t$ .

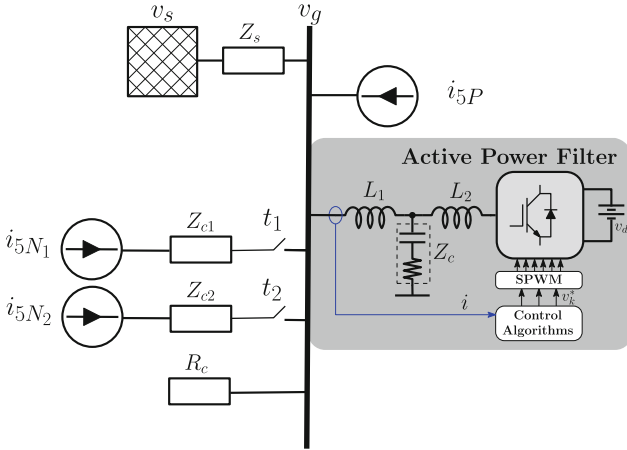


**Fig. 1.** Simplified electrical diagram of the simulated circuit.

**Table 1.** Summarized parameters of the simulated circuit - Fig. 1.

Item	Symbol	Value
Grid impedance	$Z_S$	130 $\mu\text{H}$
Converter-side filter inductor	$L_2$	250 $\mu\text{H}$
Grid-side filter inductor	$L_1$	300 $\mu\text{H}$
RC branch impedance	$Z_C$	$R_1 = 5 \Omega$ & $C_1 = 10 \mu\text{F}$
Harmonic load 1	$Z_{c1}$	$R_{c1} = 0.6 \Omega$ & $L_{c1} = 3.7 \text{ mH}$
Harmonic load 2	$Z_{c2}$	$R_{c2} = 1.4 \Omega$ & $L_{c2} = 8.9 \text{ mH}$
Three-phase load resistance	$R_c$	5 $\Omega$
Harmonic current source 1	$I_{5P}$	5 A
Harmonic current source 2	$I_{5N1}$	15 A
Harmonic current source 3	$I_{5N2}$	5 A

In sequence, the compensation algorithm determines the reference currents,  $ia_{5h}^*, ib_{5h}^*, ic_{5h}^*$ . Finally, there is a controller to ensure that the power-converter currents ( $i_{fa}, i_{fb}, i_{fc}$ ) correspond to the reference ones, with  $C_i(S)$  corresponding to a proportional gain and  $v_a^*, v_b^*, v_c^*$  modulated through pulse width modulation (PWM) switching technique.

### 3.1 Proposed Compensation Algorithm

The proposed compensation algorithm can be divided into 2 stages, comprehended by the cost-function -and optimization-algorithms. The output of the cost-function corresponds to the control signal  $|V_g|$  and it is determined as follows:

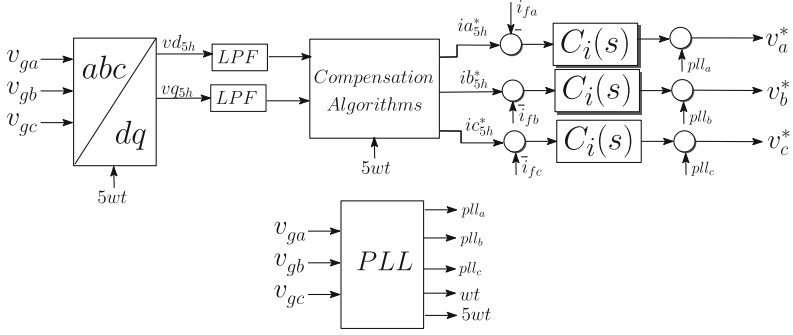


**Fig. 2.** Simplified block diagrams of the implemented algorithms.

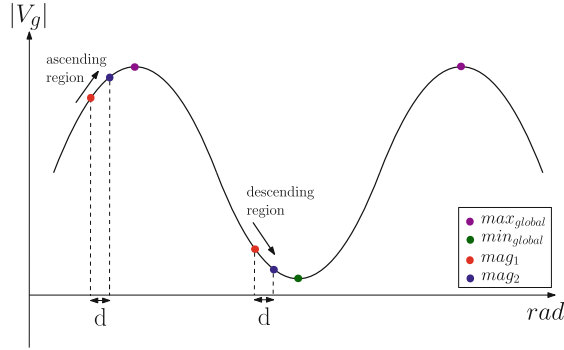


**Fig. 3.** Cost function for a cycle period of the phase angle  $\delta$ .

$$|V_g| = \sqrt{Vd_{5h}^2 + Vq_{5h}^2} \quad (1)$$

The control signals  $Vd_{5h}$  and  $Vq_{5h}$  are the average components of  $vd_{5h}$  and  $vq_{5h}$ , respectively. As an example,  $|V_g|$  is decreased to zero if fully compensation of the selected harmonic current was considered. Nevertheless, considering the limited capacity of the power converter to provide fully compensation, optimization algorithms were used to identify the phase-angle of the selected harmonic component that leads  $|V_g|$  to its minimum value, being constant the magnitude of the reference currents. Figure 3 illustrates the cost function for a cycle period of  $\delta$ , being  $\delta$  the phase angle of the reference currents. In this case, the angular frequency ( $\omega t$ ) was previously determined by the PLL circuit whereas the magnitude was considered constant and equal to 10 A. Moreover, it was considered that the resultant amplitude of the fifth-harmonic components drawn by the non linear loads were always higher than 10 A. Taken into account these conditions, the optimization method was implemented.

According to the cost function illustrated in Fig. 3 one may note 2 critical points, corresponding to the maximum -and minimum-values of  $|V_g|$ . Our objective is to identify the phase-angle that leads  $|V_g|$  to its minimum value. Thus,

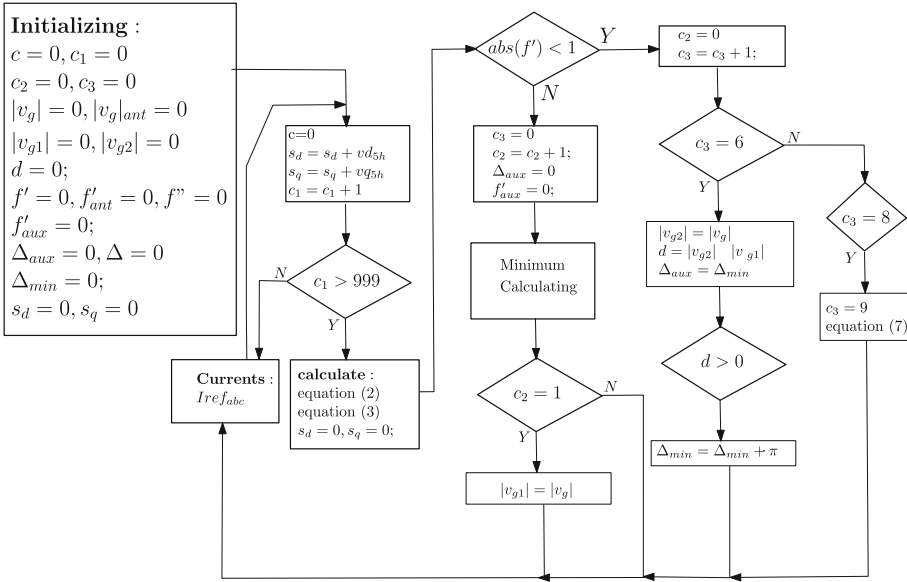


Fig. 4. Flow chart of the proposed algorithm.

to solve this problem an optimization method must consider the gradient signal of the cost function. Indeed, a positive gradient signal, or ascending region indicated in Fig. 3, indicates the cost function at its maximum. In sequence, further details of the implemented optimization method are explained with the help of a flowchart illustrated in Fig. 4.

The flow chart can be divided into three steps: initially,  $|V_g|$  and its corresponding derivative signal ( $f'$ ) were calculated as follows:

$$|V_g| = \sqrt{\left(\frac{S_d}{1000}\right)^2 + \left(\frac{S_q}{1000}\right)^2}; \tag{2}$$

$$S_d = \sum_{n=1}^{1000} V d_{5h-n}; \tag{3}$$

$$S_q = \sum_{n=1}^{1000} V q_{5h-n}; \tag{4}$$

$$f' = |V_g| - |V_{g\_ant}| \tag{5}$$

It is important to comment that 1000 samples correspond to a 1.5 cycle period of the fundamental frequency ( $\omega t$ ), or 9 cycle periods of  $6 \omega t$ , which remains as the oscillating component in the control signals  $vd_{5h}$  and  $vq_{5h}$ . In sequence the identification of the minimum region of the cost function was performed. It was done combining a minimization method with the corresponding

gradient signal of the cost function. It was implemented 2 minimization methods (Newton-Raphson and secant) to evaluate the performance of the proposed algorithm. The gradient signal was determined based on the difference between 2 samples of  $|V_g|$ , one acquired at steady state condition and the other one corresponds to the first sample acquired. The steady state condition was assumed when the derivative signal remains inside a bandwidth region for a minimal time period, which corresponds to 9 cycle periods of the fundamental frequency. In this condition is assured that the cost function is at its minimum with the reference currents given by:

$$\begin{cases} ia_{5h}^* = 10\sin(5\omega t + \Delta_{min}) \\ ib_{5h}^* = 10\sin(5\omega t + 2\pi/3 + \Delta_{min}) \\ ic_{5h}^* = 10\sin(5\omega t - 2\pi/3 + \Delta_{min}) \end{cases} \quad (6)$$

One may note that the steady state condition is remained while the derivative signal of the cost function is inside of the bandwidth region. Furthermore, it is important to comment that this method is able to identify the global minimum point or global maximum point, which could be applied to tracker of the Maximum Power Point (MPPT) algorithms for instance [19].

**Implementation of the Minimization Methods.** Essentially, the Newton-Raphson method is based on the simple idea of linear approximation, as described through Eqs. 7 and 8.

As explained in the previous sections, once determined a critical point of the cost function, is also possible to identify if the critical point corresponds to the maximum or minimum value of the cost function. Indeed, once the cost function is similar to the sine or cosine functions, if  $f''(x_n) > 0$  then  $f(x_n)$  is a local (or global) minimum. On the other hand, if  $f''(x_n) < 0$  then  $f(x_n)$  is a local maximum. This method is repeated while the absolute value of the cost function ( $f'(x_n)$ ) remains higher than the stop criteria value.

$$f''(x_n) = f'(x_n) - f'(x_{n-1}) \quad (7)$$

$$x_{n+1} \approx x_n - \frac{f'(x_n)}{f''(x_n)} \quad (8)$$

The Secant Method starts with two estimates of the root,  $x_0$  and  $x_1$ , and can be interpreted as a method in which the derivative is replaced by an approximation and is thus a quasi-Newton method. For  $n \geq 1$ , the iterative function is described in the Eq. 9 as follows.

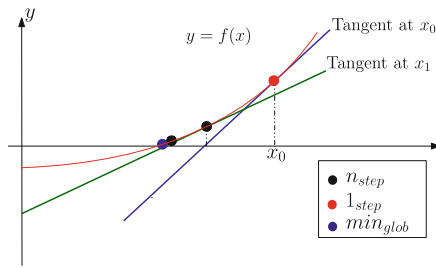
For  $n = 1, 2, \dots$ , until the stopping criteria is achieved,

1. Compute  $f(x_n)$  and  $f(x_{n-1})$
2. Compute the next approximation:  $x_{k+1}$

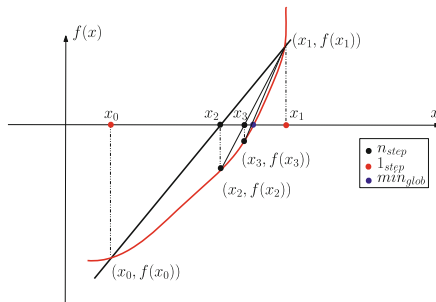
3. Test for convergence or maximum number of iterations: If  $|x_{k+1}x_k| < tolerance$  or if  $k > N$

$$\begin{aligned}
 x_n &= x_{n-1} - f(x_{n-1}) \frac{x_{n-1} - x_{n-2}}{f(x_{n-1}) - f(x_{n-2})} \\
 x_n &= \frac{x_{n-2}f(x_{n-1}) - x_{n-1}f(x_{n-2})}{f(x_{n-1}) - f(x_{n-2})}
 \end{aligned}
 \tag{9}$$

If we compare secant method with the Newton-Raphson, one may note that Newton-Raphson converges faster than secant method. However, secant method only requires the evaluation of  $f$ , while the Newton's method requires the evaluation of both  $f$  and its derivative  $f'$  at every step. Therefore, the secant method may occasionally be faster in practice (Fig. 5).



(a)



(b)

**Fig. 5.** (a) Geometric interpretation of the Newton-Raphson iteration, (b) Geometric interpretation of the Secant iteration.

## 4 Simulation Results

To verify the effectiveness of the controller with the proposed algorithm, test cases of the described circuit in Sect. 2 were carried out with PSIM simulator.



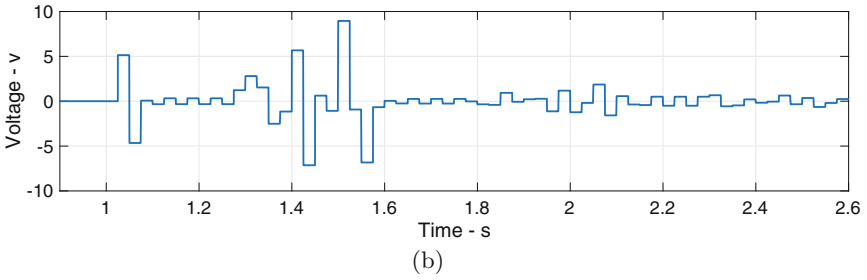
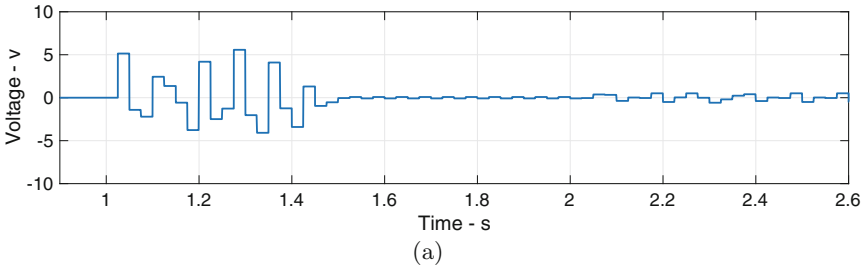
Basically, 2 test cases were performed considering the active filter performance with the control algorithms determining, dynamically, the reference currents. At each test case the reference currents were determined by a different minimization method, where the first one corresponds to Newton-Raphson, while the second corresponds to the Secant method.

In both test cases, the simulation starts with the active power filter (APF) turned-off, and all of the control algorithms disabled. At  $t_1 = 0.5$  s and  $t_2 = 2.0$  s, the first -and the second-loads were turned-on as follows. It is important to comment that the drawn currents by these loads are identified in Fig. 1 as  $i_{5N1}$  and  $i_{5N2}$ , respectively. Moreover,  $i_{5P}$  was not compensated once the control algorithm was configured to compensate only the negative-sequence fifth-harmonic currents. The active filter was turned-on at  $t = 1.0$  s, and the algorithms of the reference currents were enabled.

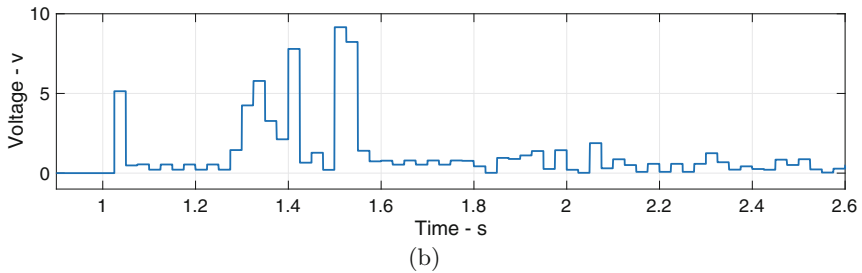
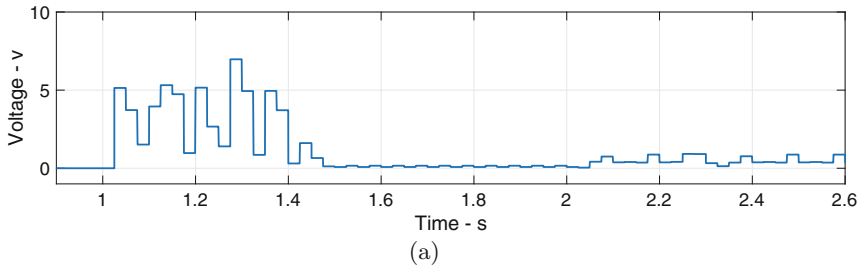
Transient response of the control algorithm based on Newton-Raphson -and Secant-methods are shown from Figs. 6, 7, 8, 9, 10, 11, 12 and 13. Initially, the derivative waveform of the cost function with Newton-Raphson -and Secant-methods are depicted at Fig. 6(a) and (b), respectively. One may note a smooth behavior at Fig. 6(a) with a faster convergence, indicating a better performance of the algorithm based on the Newton-Raphson method. Nevertheless, with both methods, the gradient of the cost function decreased to zero, indicating, initially, that a critical point was reached.

In sequence, the cost function waveform with the control algorithm based on the Newton-Raphson -and Secant-methods are shown in Fig. 7(a) and (b), respectively. Based on these results, the cost function was decreased to its minimum, with Fig. 7(a) presenting a smooth behavior and a faster convergence. Furthermore, one may note that, initially, the harmonic currents were entirely compensated once the cost function was decreased close to zero. In sequence, when the second load was turned-on, it was no longer possible to provide fully compensation of the harmonic currents due to the limited capacity of the power converter. This condition leads to note a correct performance of the proposed algorithm. Next, the average components of direct -and quadrature-voltages with the control algorithm based on Newton-Raphson -and Secant-methods are illustrated in Fig. 8(a) and (b), respectively.

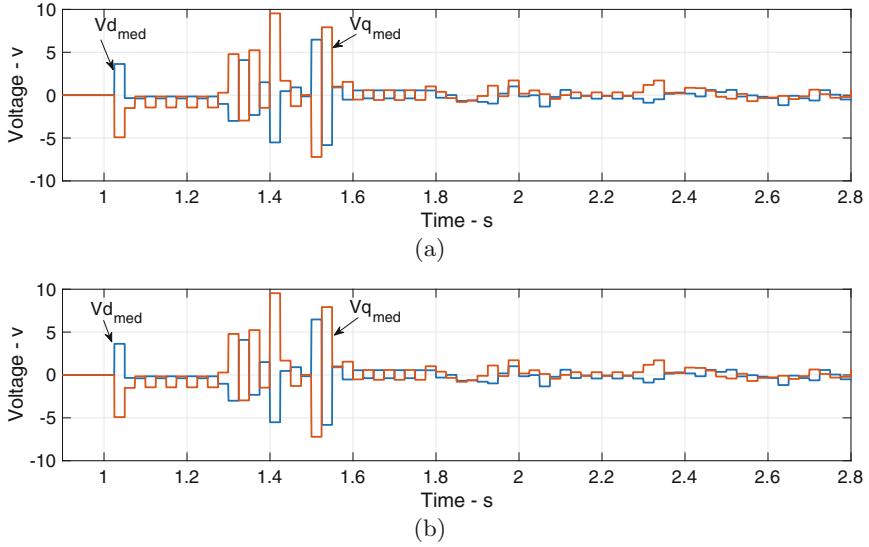
Figure 9 presents the grid current,  $ia_{source}$ , and the active filter current,  $ia_{filter}$ , during the entire simulation. Based on the previous results, both algorithms were capable to minimize the distorted load-currents and, as expected, one can see a decrement of  $ia_{source}$  when both algorithms reached their steady-state condition. At  $t = 2.0$  s, when the second harmonic turned-on, it was no possible to provide full compensation due to the limited capacity of the power converter and, therefore,  $ia_{source}$  has increased. Moreover, as observed at the previous results, the algorithm based on the Newton-Raphson method (Fig. 9(a)) presented a faster transient convergence reaching a steady-state condition at, approximately,  $t = 1.4$  s whereas, with the Secant method (Fig. 9(b)) the steady-state condition was reached at  $t = 1.5$  s. In the second transient, both methods presented a similar performance.



**Fig. 6.** Derivative waveform of the cost function with (a) Newton-Raphson method and (b) Secant method.



**Fig. 7.** Cost function waveform with minimization algorithms based on (a) Newton-Raphson method and (b) Secant method.



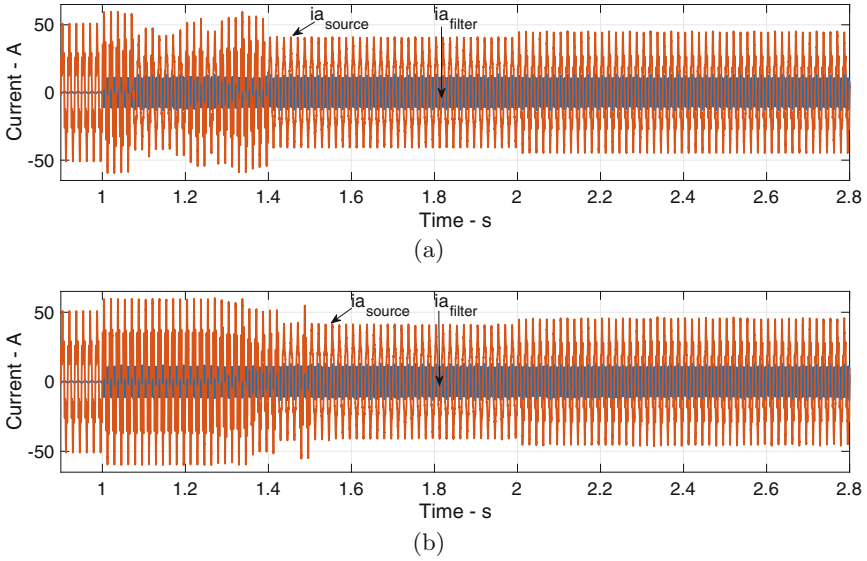
**Fig. 8.** Average components of the direct -and quadrature-voltages with (a) Newton-Raphson method and (b) Secant method.

Figure 10 illustrates the grid current,  $ia_{source}$ , active-filter current,  $ia_{filter}$ , and load current,  $ia_{load}$ , during the transient when the active filter was turned-on with Newton-Raphson method (Fig. 9(a)) and Secant method (Fig. 9(b)). In this transient  $ia_{filter}$  was in phase with  $ia_{load}$  and, as a consequence,  $ia_{source}$  has increased. It is important to comment that  $ia_{load}$  refers to the equivalent fifth-harmonic current drawn by the nonlinear loads.

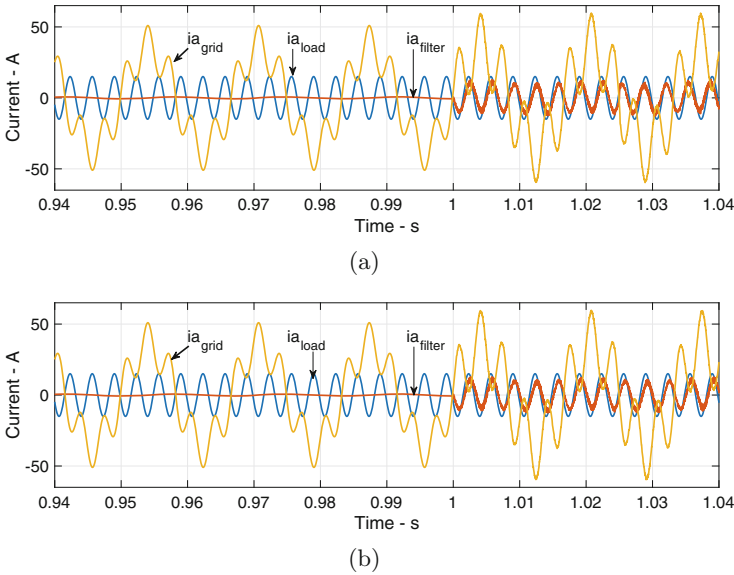
Figure 11 illustrates the grid current,  $ia_{source}$ , active-filter current,  $ia_{filter}$ , and load current,  $ia_{load}$ , during the first steady-state condition with Newton-Raphson method (Fig. 11(a)) and Secant method (Fig. 11(b)). As expected, in this condition  $ia_{filter}$  was in counter-phase with  $ia_{load}$  and, as a consequence,  $ia_{source}$  has decreased. Furthermore, once the amplitudes of  $ia_{load}$  and  $ia_{filter}$  are similar, the active filter was capable to compensate, practically, the entire harmonic content.

Figure 12 illustrates the grid current,  $ia_{source}$ , active-filter current,  $ia_{filter}$ , and load current,  $ia_{load}$ , during the transient when the second nonlinear load was turned-on. With both algorithms the active filter presented similar performance once the equivalent phase-angle of the nonlinear loads was not modified, as shown in Fig. 12(a) and (b). Nevertheless, even at this transient both algorithms were enabled once the cost-function gradient was no longer within the bandwidth region.

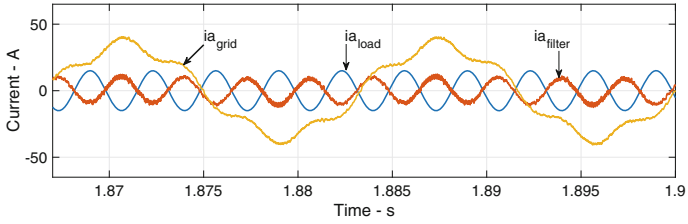
Finally, Fig. 13 illustrates the grid current,  $ia_{source}$ , active-filter current,  $ia_{filter}$ , and load current,  $ia_{load}$ , during the second steady-state condition with Newton-Raphson method (Fig. 13(a)) and Secant method (Fig. 13(b)). Again, as expected, in this condition  $ia_{filter}$  was in counter-phase with  $ia_{load}$ , however,



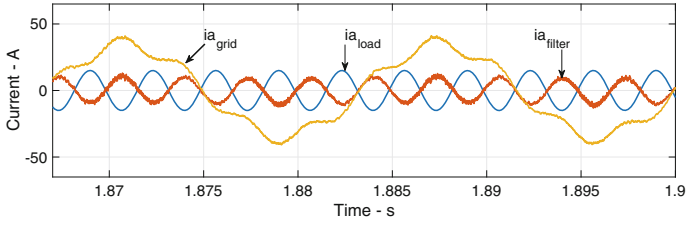
**Fig. 9.** Grid current,  $i_{a\_source}$ , and active-filter current,  $i_{a\_filter}$ , during the entire simulation with (a) Newton-Raphson method (b) Secant method.



**Fig. 10.** Grid current,  $i_{a\_source}$ , active-filter current,  $i_{a\_filter}$ , and load current,  $i_{a\_load}$ , during the transient when the active filter was turned-on with (a) Newton-Raphson method (b) Secant method.

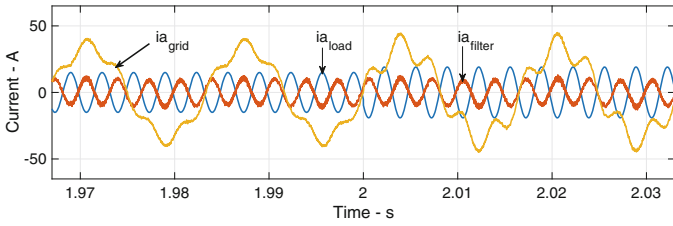


(a)

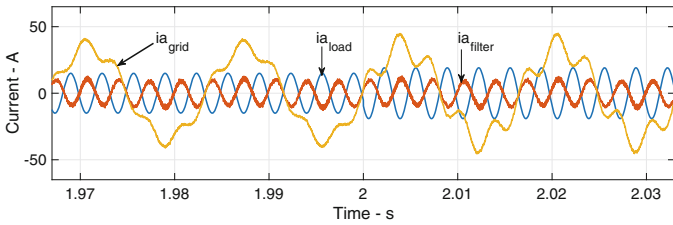


(b)

**Fig. 11.** Grid current,  $ia_{source}$ , active-filter current,  $ia_{filter}$ , and load current,  $ia_{load}$ , in the first steady-state condition with (a) Newton-Raphson method (b) Secant method.



(a)



(b)

**Fig. 12.** Grid current,  $ia_{source}$ , and active-filter current,  $ia_{filter}$ , and load current,  $ia_{load}$ , at the transient when the second nonlinear load was turned-on with (a) Newton-Raphson method (b) Secant method.

due to the limited capacity of the power converter for compensating the entire harmonic current,  $ia_{source}$  has increased. Nevertheless, this result reinforces the correct operation of the proposed algorithm for providing the best harmonic filtering within its limitations.

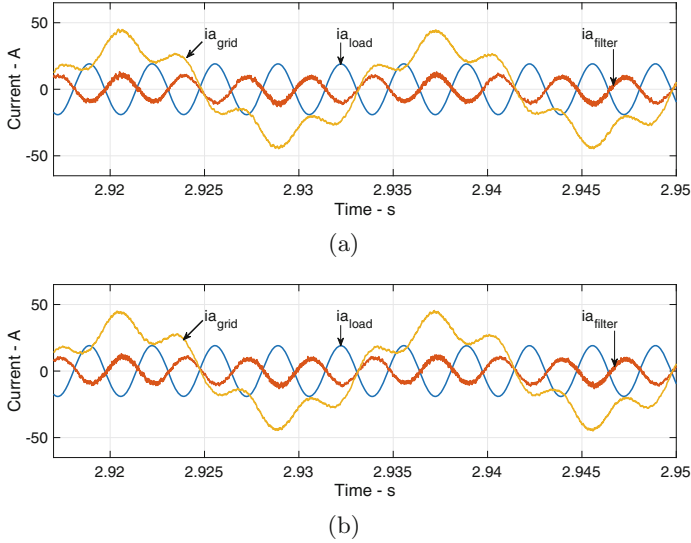


**Fig. 13.** Grid current,  $ia_{source}$ , active-filter current,  $ia_{filter}$ , and load current,  $ia_{load}$ , in the second steady-state condition with (a) Newton-Raphson method (b) Secant method.

## 5 Conclusions

It is important to note that there are other techniques that can identify the global minimum point and correctly trace the harmonic current, such as those presented by [12–14, 16, 18].

Based on the results of the simulation, the ability of the proposed algorithm to identify the global minimum point after a disturbance occurred and to maintain it at steady-state was verified, even after new disturbances. Thus, it is capable of correctly tracking the frequency and phase-angle of the selected harmonic current. Nevertheless, it is important to point out that we assumed that the produced current by the active filter was always lower than the selected harmonic currents and this condition is not necessarily true.

To the future works, other global optimization algorithms will be explored and compared with the algorithm introduced in this work, considering other test cases such as use of variable network impedance, harmonic current tracking when the harmonic current source is disconnected of the power grid. These questions will be explored in the future work, as well as the evaluation of the algorithm proposed through experimental results.

## References

1. Wu, C.H., et al.: Investigation and mitigation of harmonic amplification problems caused by single-tuned filters. *IEEE Trans. Power Deliv.* **13**(3), 800–806 (1998)
2. Dao, T., Phung, B.T.: Effects of voltage harmonic on losses and temperature rise in distribution transformers. *IEE Proc. - IET Gener. Transm. Distrib.* **12**(2), 347–354 (2017)
3. Nishida, K., Rukonuzzman, M., Nakaoka, M.: Advanced current control implementation with robust deadbeat algorithm for shunt single-phase voltage-source type active power filter. *IEE Proc. - Electr. Power Appl.* **151**(3), 283–288 (2004)
4. Akagi, H., Nabae, A., Atoh, S.: Control strategy of active power filters using multiple voltage-source PWM converters. *IEEE Trans. Ind. Appl.* **IA-22**(3), 460–465 (1986)
5. Aredes, M., Watanabe, E.H.: New control algorithms for series and shunt three-phase four-wire active power filters. *IEEE Trans. Ind. Appl.* **10**(3), 1649–1656 (1995)
6. Mattavelli, P.: A closed-loop selective harmonic compensation for active filters. *IEEE Trans. Ind. Appl.* **37**(1), 81–89 (2001)
7. Yuan, X., Merk, W., Stemmler, H., Allmeling, J.: Stationary-frame generalized integrators for current control of active power filters with zero steady-state error for current harmonics of concern under unbalanced and distorted operating conditions. *IEEE Trans. Ind. Appl.* **38**(2), 523–532 (2002)
8. Miret, J., Castilla, M., Matas, J., Guerrero, J.M., Vasquez, J.C.: Selective harmonic-compensation control for single-phase active power filter with high harmonic rejection. *IEEE Trans. Ind. Electron.* **56**(8), 3117–3127 (2009)
9. Trinh, Q., Lee, H.: An advanced current control strategy for three-phase shunt active power filters. *IEEE Trans. Ind. Electron.* **60**(12), 5400–5410 (2013)
10. Morales, J., et al.: Modeling and sliding mode control for three-phase active power filters using the vector operation technique. *IEEE Trans. Ind. Electron.* **65**(9), 6828–6838 (2018)
11. Akagi, H.: Active harmonic filters. *Proc. IEEE* **93**12, 2128–2141 (2005)
12. Lee, T., Tzeng, K., Chong, M.: Fuzzy iterative learning control for three-phase shunt active power filters. In: 2006 IEEE International Symposium on Industrial Electronics (2006)
13. Luo, A., et al.: Feedback-feedforward PI-type iterative learning control strategy for hybrid active power filter with injection circuit. *IEEE Trans. Ind. Electron.* **57**(11), 3767–3779 (2010)
14. Kukkola, J., Hinkkanen, M.: State observer for grid-voltage sensorless control of a converter under unbalanced conditions. *IEEE Trans. Ind. Appl.* **54**(1), 286–297 (2018)
15. Bai, H., Wang, X., Blaabjerg, F.: A grid-voltage-sensorless resistive-active power filter with series LC-filter. *IEEE Trans. Power Electronics* **33**(5), 6828–6838 (2018)
16. Monteiro, L.F.C., Encarnação, L.F., Aredes, M.: A novel selective control algorithm for the shunt active filter. In: IEEE International Power Electronics Conference, pp. 2288–2293 (2010)
17. Freitas, C.M., Do Nascimento, C.R., Bellar, M.D., Monteiro, L.F.C.: Control algorithms for a transformerless hybrid active filter without current sensors. In: 40th Annual Conference of the IEEE Industrial Electronics Society, pp. 5163–5168 (2014)

18. Freitas, C.M., Monteiro, L.F., Watanabe, E.H.: A novel current harmonic compensation based on resonant controllers for a selective active filter. In: 42nd Annual Conference of the IEEE Industrial Electronics Society, pp. 3666–3671 (2016)
19. Macellari, M., Grasselli, U., Schirone, L.: Modular MPPT converter with series-connection for PV installations embedded in the urban environment. In: IECON 2013–39th Annual Conference of the IEEE Industrial Electronics Society, pp. 1755–1760 (2013)